Atomic Level Control over Surface Species via a Molecular Precursor Approach: Isolated Cu(I) Sites and Cu Nanoparticles Supported on Mesoporous Silica

Kyle L. Fujdala,[†,‡] Ian J. Drake,[§] Alexis T. Bell,[‡,§] and T. Don Tilley*,[†,‡]

Departments of Chemistry and Chemical Engineering, University of California, Berkeley, Berkeley, California 94720, and Chemical Sciences Division, Lawrence Berkeley National Laboratory, 1 Cyclotron Road, Berkeley, California 94720
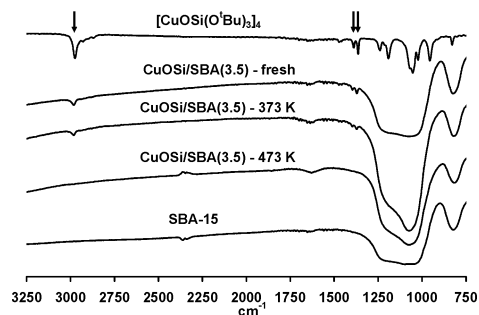
Received March 6, 2004; E-mail: tdtilley@socrates.berkeley.edu

There is a growing interest in the preparation of catalysts with well-defined and isolated sites, as such systems are ideally suited for structure−function investigations.[1] Recent studies indicate that atomically dispersed metals on high surface area silica materials are effective catalysts.[2−4] Thus, an important goal in catalysis research is the development of synthetic methods that provide atomic-level control over the nature of catalytic sites, with formation of isolated single sites or homogeneously distributed and more complicated structures (bimetallic sites, clusters, nanoparticles, etc.) providing new and improved catalysts.[1−4] It is believed that low-temperature approaches will be most effective for generating tailored structures because of the metastable nature of many of the desired structures.[1]

Supported Cu-containing catalysts have been studied for a number of industrially relevant reactions,[5−8] but little effort has been devoted to the generation of tailored sites. The introduction of isolated species onto mesoporous silica using molecular precursors of the form $M[OSi(O^tBu)_3]_n$ (M = Ti[3a] and Fe[3b]) under nonaqueous conditions has recently been reported. The work presented herein provides direct evidence for atomic-level control over the nature of sites that result from grafting[9] Cu-containing molecular precursors onto the mesoporous silica SBA-15.[10]

Reaction of the molecular precursors $[CuOSi(O^tBu)_3]_4$[11] (**1**) or $[CuO^tBu]_4$[12] (**2**) (as solutions in C_6H_6) with the surface hydroxyl groups of SBA-15 under inert conditions provided grafted materials, isolated as light yellow powders after extensive washing with C_6H_6 and drying in vacuo at 323 K. Quantities of the molecular precursors were used such that the final grafted materials contained ca. 3.5% (**CuOSi/SBA(3.5)** and **CuO^tBu/SBA(3.5)** from **1** and **2**, respectively) and ca. 5.0% (**CuOSi/SBA(5.0)** and **CuO^tBu/SBA(5.0)** from **1** and **2**, respectively) Cu by weight.[13] It is known that $M[OSi(O^tBu)_3]_n$ species cleanly evolve $3nCH_2C(CH_3)_2$ and $^3/_2nH_2O$ upon mild thermolysis (373 to 473 K) to give MSi_nO_y materials.[1a,14] Previous studies of **1** indicate that it also exhibits loss of $CH_2C(CH_3)_2$ and H_2O upon heating, although some reduction of Cu (to Cu metal) is evident under an inert atmosphere.[11] It was anticipated that grafting **1** onto SBA-15 would provide species that could eliminate $CH_2C(CH_3)_2$ and H_2O upon thermolysis to form Si−O surface linkages while maintaining some of the original Cu−O−Si linkages to provide stabilized Cu(I) species (in the form of isolated tetramers or as single sites). Use of **2** in similar grafting reactions may also provide isolated sites; however, no additional Si−O surface linkages (and hence extra site stabilization) are provided by this precursor. Scheme 1 illustrates a possible grafting pathway and potential structure types for the resulting surface species.

The molecular precursors are presumably well-separated on the surface, as the "OH" site-to-precursor ratios are 12:1 and 8:1 for the

† Department of Chemistry, University of California.
‡ Lawrence Berkeley National Laboratory.
§ Department of Chemical Engineering, University of California.

Figure 1. IR spectra of **CuOSi/SBA(3.5)**, uncalcined and after thermal treatments for 1 h under N_2. IR spectra of **1** and SBA-15 are also shown. The arrows indicate bands from the $-OSi(O^tBu)_3$ ligands.

Scheme 1
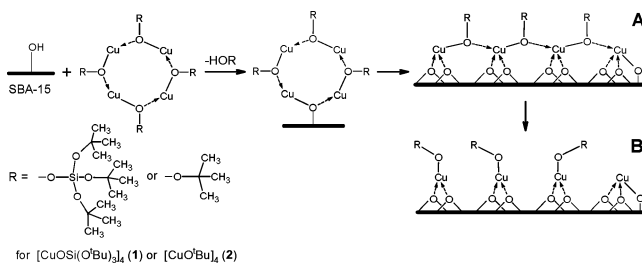
3.5 and 5.0 wt % materials, respectively.[15] The reaction of **1** with the hydroxyl groups of the SBA-15 proceeds via loss of only 1 equiv of $HOSi(O^tBu)_3$ per $[CuOSi(O^tBu)_3]_4$ tetramer (with no ^tBuOH observed), as shown by ^1H NMR studies (C_6D_6) of the reaction in situ and of the soluble reaction products obtained after isolation and washing of the materials. Further, thermogravimetric analysis (TGA) of **CuOSi/SBA(3.5)** reveals a mass loss of 7.77% below 673 K, corresponding closely to that predicted for loss of the appropriate quantities of $CH_2C(CH_3)_2$ and H_2O from three Cu−O−Si(O^tBu)_3 linkages per molecule of **1** (7.91%). Additionally, IR studies of **CuOSi/SBA(3.5)** reveal bands due to $-OSi(O^tBu)_3$ groups[14] that are lost upon heating under N_2 at 473 K (Figure 1). Grafting reactions using **2** are also clean, and evolve 1 equiv of ^tBuOH per grafted molecule, as shown by ^1H NMR studies. Also, an observed mass loss of 3.70% upon heating **CuO^tBu/SBA(5.0)** (by TGA) is in close agreement with the loss predicted for evolution of $CH_2C(CH_3)_2$ and H_2O (4.14%) from three O^tBu groups per molecule of **2**.

As expected, the grafted materials have surface areas and pore volumes that are reduced relative to that of the SBA-15 support (894 $m^2 g^{-1}$ and 1.13 $cm^3 g^{-1}$); however, the mesostructured nature was maintained. The reduction in surface area and pore volume was proportional to the amount and size of the molecular precursor used, with **CuOSi/SBA(5.0)** exhibiting the most dramatic decrease.[16] The surface areas and pore volumes of the grafted materials

Table 1. XANES Edge Energies and EXAFS FEFF Fitting Results

| Material	XANES E_0 (eV)[a]	Shell	CN[b]	R (Å)[c]	σ^2 (Å²)[d]	E_0 (eV)[e]	ℜ-factor[f]
CuO^{t}Bu/SBA(3.5)	8982.3	**Cu–O**	3.6(2)	1.928(4)	0.0041(5)	-1.4(7)	0.0047
		Cu–Cu	2.1(2)	2.87(1)	0.013[j]		
CuO^{t}Bu/SBA(5.0)	8981.7	**Cu–O**	3.4(2)	1.925(4)	0.0055(6)	2.2(8)	0.0056
		Cu–Cu	1.8(2)	2.86(1)	0.013[j]		
CuOSi/SBA(3.5)	8982.1	**Cu–O**	2.4(2)	1.877(8)	0.004(1)	1.5(1.5)	0.0262
		Cu–Si	0.7(7)[i]	3.11(4)	0.006(9)		
CuOSi/SBA(5.0)	8980.7	**Cu–O**	2.9(1)	1.895(4)	0.0051(5)	1.9(7)	0.0061
		Cu–Si	1.5(5)[i]	3.12(1)	0.009(4)		
CuO^{t}Bu/SBA(3.5) (heated)	8979.4	**Cu–Cu**	7.8(3)	2.52(2)	0.0062(9)	3.0(5)	0.0025
		Cu–Cu	4.7(2.6)	3.57(2)	0.012(4)		
		MS1[g]	22(16)	3.79(2)	0.01[j]		
CuO^{t}Bu/SBA(5.0) (heated)	8979.5	**Cu–Cu**	7.6(3)	2.52(1)	0.0072(3)	1.5(6)	0.0021
		Cu–Cu	4.2(2.9)	3.58(1)	0.013(5)		
		MS1[g]	18(14)	3.80(1)	0.01[j]		
CuOSi/SBA(3.5) (heated)	8981.7	**Cu–O**	1.9(3)	1.85(1)	0.003(1)	0.3(2.4)	0.0261
		Cu–Cu[h]	0.7(6)	2.55(2)	0.007(5)		
CuOSi/SBA(5.0) (heated)	8980.7	**Cu–O**	1.7(1)	1.851(6)	0.0029(7)	1.4(1.3)	0.0249
		Cu–Cu[h]	1.2(3)	2.54(1)	0.007(1)		

[a] Edge energy defined as the first inflection point on the rising absorption edge. E_0 for standards: Cu foil, 8980.0 eV; Cu₂O, 8980.8 eV; **1**, 8982.1 eV; **2**, 8981.5 eV; CuO, 8984.5 eV. [b] Coordination number. [c] Fitted radial distance. [d] Debye–Waller factor. [e] Energy reference shift relative to the XANES edge energy. [f] The ℜ factor gives a sum-of-square measurement of the fractional misfit. [g] The first significant multiscattering path, with R = half the total scattering distance. [h]Cu–Si scattering could not be separated. [i] Large errors are due to the amorphous support and a wide variation in Cu–O–Si(O^{t}Bu)₃ bond angles. [j] Fixed value.

increased (all to similar values) upon heating at 673 K under N_2 because of loss of the organic groups.[16]

The local environment of Cu in the grafted materials was characterized by X-ray absorption near-edge structure (XANES) and extended X-ray absorption fine structure (EXAFS) analyses before (uncalcined) and after heating (He, 573 K, 1 h). The signal-to-noise ratios and overall quality of the spectra were good for all samples and standards.[17] Analyses of EXAFS data were carried out using information obtained from a series of well-defined standards, including the molecular precursors **1** and **2**. The XANES spectra of the standards (Cu foil, Cu₂O, **1**, **2**, and CuO) and the grafted materials are provided in the Supporting Information. The XANES edge energies observed for all of the uncalcined materials lie in the range characteristic for Cu(I) species (8980.5–8982.5; Table 1).[18]

The molecular precursor **1** proved to be an excellent model for Cu species on silica materials, providing clear identification of Cu–Si and Cu–Cu next-nearest neighbor interactions by analysis of the imaginary part of the FT $k^3\chi(k)$ spectrum.[17] Use of **2** as a model compound provided additional data for the assignment of Cu–Cu next-nearest-neighbor interactions. The EXAFS fitting results for the uncalcined materials are presented in Table 1. The FT $k^3\chi(k)$ spectra for the uncalcined materials are shown in Figure 2a,b together with representative best fit spectra. Each spectrum has a prominent Fourier component centered between 1.47 and 1.53 Å, attributed to Cu–O backscattering. The average Cu–O coordination numbers (CNs) for uncalcined **CuOSi/SBA(3.5)** and **CuOSi/SBA-(5.0)** were lower than those for uncalcined **CuO^{t}Bu/SBA(3.5)** and **CuO^{t}Bu/SBA(5.0)**, suggesting increased Cu–O interactions for the latter materials (Table 1).

The interpretation of the Fourier components in Figure 2a,b appearing at 2.5 Å was aided by examination of the imaginary part of their respective FT $k^3\chi(k)$ spectra. The magnitude and imaginary parts of the forward FT $k^3\chi(k)$ spectra for uncalcined **CuO^{t}Bu/SBA(3.5)** and **CuO^{t}Bu/SBA(5.0)** are essentially identical. The similarity in the shapes and positions of the maxima and minima for the observed and simulated imaginary components (using **2** as a model) indicates that the peak at 2.5 Å is due to Cu–Cu backscattering (Figure 2a). However, this does not preclude a Cu–Si backscattering contribution of small (undetectable) magnitude from Cu–O–Si(support) interactions. The radial separation of Cu–Cu
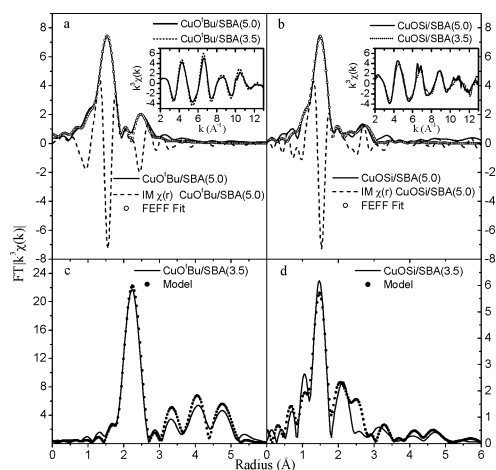
Figure 2. Nonphase-corrected FT $k^3\chi(k)$ spectra and the fitting results for (a) uncalcined **CuO^{t}Bu/SBA(5.0)** and (b) uncalcined **CuOSi/SBA(5.0)**, with the $k^3\chi(k)$ spectra for the respective 3.5 and 5.0% Cu-containing materials (inset). Nonphase-corrected FT $k^3\chi(k)$ spectra and model comparisons for (c) heated **CuO^{t}Bu/SBA(3.5)** and (d) heated **CuOSi/SBA(3.5)**. For (c), comparison is with a 55-atom Cu particle, with the FEFF calculated assuming $S_o^2 = 0.86$ and $\sigma^2 = 0.0072$ Å² for all scattering paths. For (d), comparison is with a linear combination of uncalcined **CuOSi/SBA(3.5)** and heated **CuO^{t}Bu/SBA(3.5)**.

nearest neighbors in uncalcined **CuO^{t}Bu/SBA(3.5)** and **CuO^{t}Bu/SBA(5.0)** is longer than that found for **2** (2.716(5) Å), indicating a relaxation of the Cu–O–Cu bond angles (Table 1). Thus, uncalcined **CuO^{t}Bu/SBA(3.5)** and **CuO^{t}Bu/SBA(5.0)** have primarily Cu(I)–Cu(I) next-nearest-neighbor interactions, with Cu–Si(support) contributions. Given entropic considerations, the low Cu–Cu CNs (Table 1), and the relatively high Cu–O CNs, we propose a structure involving a "relaxed" straight chain of Cu–O^{t}Bu–Cu linkages in which the ring structure of **2** has been disrupted (Scheme 1A).

The magnitude and imaginary parts of the forward FT $k^3\chi(k)$ spectra for uncalcined **CuOSi/SBA(3.5)** and **CuOSi/SBA(5.0)** are also essentially identical.[17] The dominant next-nearest-neighbor contributions for these materials are due to Cu–Si backscattering, as determined using the method described above, with **1** as a model for Cu–Si interactions (Figure 2b). There was no evidence for Cu–Cu next-nearest-neighbor interactions, despite several fitting attempts. Hence, the EXAFS data for uncalcined **CuOSi/SBA(3.5)** and **CuOSi/SBA(5.0)** indicate that the central Cu–OSi(O^{t}Bu)₃–Cu linkages of **1** are disrupted upon grafting, presumably due to the extreme bulk of the –OSi(O^{t}Bu)₃ ligands, to give an isolated structure. Two different types of isolated Cu(I) species are proposed: a Cu(I) center with a direct Si(surface)–O–Cu linkage and three Cu(I) centers with Cu–O–Si(O^{t}Bu)₃ linkages still intact from their precursor origin (Scheme 1B).

The XANES spectra of heated (He, 573 K, 1h) **CuOSi/SBA-(3.5)**, **CuOSi/SBA(5.0)**, **CuO^{t}Bu/SBA(3.5)**, and **CuO^{t}Bu/SBA(5.0)** exhibit distinct differences,[17] with the edge energies for **CuOSi/SBA(3.5)** and **CuOSi/SBA(5.0)** in the range expected for Cu(I) species[18] and those for **CuO^{t}Bu/SBA(3.5)** and **CuO^{t}Bu/SBA(5.0)** indicative of reduction to Cu(0) (Table 1).

The EXAFS analyses provided further evidence of reduction in heated **CuO^{t}Bu/SBA(3.5)** and **CuO^{t}Bu/SBA(5.0)**, in that their FT $k^3\chi(k)$ spectra have the same shape as that of Cu metal (Figure 2c), with the peaks at 2.23, 3.4, 4.1, and 4.7 Å (nonphase corrected) being attributed to the first four coordination shells in Cu metal. This, coupled with the absence of any significant Fourier component that can be assigned to Cu–O backscattering, suggests that all detectable Cu has been reduced to Cu metal. A procedure that is similar to one used for analysis of EXAFS data for carbon-supported Pt nanoparti-

cles[19] was used to determine that the ratio of average Cu−Cu CNs for the first and second shell is consistent with that reported for a 55-atom fcc cluster.[20] Hence, the Cu atoms in **CuOᵗBu/SBA(3.5)** and **CuOᵗBu/SBA(5.0)** are reduced upon heating and undergo sintering to form Cu nanoparticles with an average diameter of ca. 7 Å.

In contrast, the FT $k^3\chi(k)$ spectra of heated (He, 573 K, 1h) **CuOSi/SBA(3.5)** and **CuOSi/SBA(5.0)** exhibit a dominant Fourier component at 1.47 Å assigned to Cu−O backscattering, suggesting that the majority of the sites are still Cu(I) species associated with O (Figure 2d). Although the spectra of these heated materials exhibit peaks at 2.11, 3.34, 4.1, and 4.7 Å (associated with Cu metal), they are of small magnitude, suggesting the presence of only minor amounts of Cu metal particles (ca. 7 Å in diameter). To determine the ratio of isolated Cu(I) species versus metallic Cu in heated **CuOSi/SBA(3.5)** and **CuOSi/SBA(5.0)**, a linear combination of the experimental $k^3\chi(k)$ and FT $k^3\chi(k)$ data for heated **CuOᵗBu/SBA(3.5)** and uncalcined **CuOSi/SBA(3.5)** or **CuOSi/SBA(5.0)** was used as a model for their $k^3\chi(k)$ and FT $k^3\chi(k)$ spectra. The fraction of Cu present as isolated Cu(I) centers was determined to be ca. 88% for **CuOSi/SBA(3.5)** and ca. 79% for **CuOSi/SBA-(5.0)**. The Cu metal in these samples likely arises from the sintering of Cu atoms not associated with Si−O (surface) linkages formed upon decomposition of the −OSi(OᵗBu)₃ ligands (Scheme 1B).

The Cu−O CNs for heated **CuOSi/SBA(3.5)** and **CuOSi/SBA(5.0)** decreased by ca. 1 from those of their uncalcined counterparts, presumably from the decreased average weighting due to minor agglomeration of locally distributed Cu atoms (Table 1). When the contribution of Cu metal is removed for these heated materials, the Cu−O CNs (both 2.2(3)) are close to those of their uncalcined counterparts, suggesting similar local environments for the isolated Cu(I) species.

It is clear that, for the materials prepared via the grafting approach using [CuOSi(OᵗBu)₃]₄ (**1**), significant stabilization of isolated Cu-(I) species is provided after loss of the organic groups from the −OSi(OᵗBu)₃ ligands and the subsequent anchoring of Si to the support via Si(surface)−O−Si linkages. It has been proposed that such extra stabilization may occur for grafted M[OSi(OᵗBu)₃]$_x$ species; however, direct evidence of such an effect has not been previously observed.[3] Use of **1** as a Cu precursor provides only isolated Cu(I) sites (100% of the Cu detected) for the uncalcined materials and maintains isolated Cu(I) sites after heating at 673 K (up to 88% of the detected Cu). In contrast, use of **2** in identical grafting and heating procedures provides isolated tetrameric Cu species (with Cu−O−Cu linkages) in the uncalcined materials (100% of detected Cu) and Cu metal nanoparticles after heating (100% of detected Cu). Thus, proper selection of the metal source and treatment conditions can give sites with tailored structures and properties, allowing for atomic-level control. Future reports will compare the materials reported here with those obtained via previously reported methods. Additional studies will describe results pertaining to the catalytic partial oxidation of methanol.

Supporting Information Available: Experimental details and additional XAS data. This material is available free of charge via the Internet at http://pubs.acs.org.

References

(1) (a) Fujdala, K. L.; Tilley, T. D. *J. Catal.* **2003**, *216*, 265−275 and references therein. (b) De Vos, D. E.; Dams, M.; Sels, B. F.; Jacobs, P. A. *Chem. Rev.* **2002**, *102*, 3615−3640. (c) Thomas, J. M. *Top. Catal.* **2001**, *15*, 85−91. (d) Basset, J.-M.; Lefebvre, F.; Santini, C. *Coord. Chem. Rev.* **1998**, *178*, 1703−1723.

(2) (a) Vidal, V.; Théolier, A.; Thivole-Cazat, J.; Basset, J.-M.; Corker, J. *J. Am. Chem. Soc.* **1996**, *118*, 4595−4602. (b) Vidal, V.; Théolier, A.; Thivole-Cazat, J.; Basset, J.-M. *Science* **1997**, *276*, 99−102.

(3) (a) Jarupatrakorn, J.; Tilley, T. D. *J. Am. Chem. Soc.* **2002**, *124*, 8380−8388. (b) Nozaki, C.; Lugmair, C. G.; Bell, A. T.; Tilley, T. D. *J. Am. Chem. Soc.* **2002**, *124*, 13194−13203.

(4) (a) Sheldon, R. A.; Wallau, M.; Arends, I. W. C. E.; Schuchardt, U. *Acc. Chem. Res.* **1998**, *31*, 485−493. (b) Murugavel, R.; Roesky, H. W. *Angew. Chem., Int. Ed. Engl.* **1997**, *36*, 477−479. (c) Maschmeyer, T.; Rey, F.; Sanker, G.; Thomas, J. M. *Nature* **1995**, *378*, 159−162. (d) Khouw, C. B.; Dartt, C. B.; Labinger, J. A.; Davis, M. E. *J. Catal.* **1994**, *149*, 195−205. (e) Tanev, P. T.; Chibwe, M.; Pinnavaia, T. J. *Nature* **1994**, *368*, 321−323. (f) Raja, R.; Thomas, J. M.; Jones, M. D.; Johnson, B. F. G.; Vaughan, D. E. W. *J. Am. Chem. Soc.* **2003**, *125*, 14982−14983.

(5) MeOH synthesis: (a) Fisher, I. A.; Bell, A. T. *J. Catal.* **1997**, *172*, 222−237. (b) Meitzner, G.; Iglesia, E. *Catal. Today* **1999**, *53*, 433−441.

(6) NO decomposition: Groothaert, M. H.; van Bokhoven, J. A.; Battiston, A. A.; Weckhuysen, B. M.; Schoonheydt, R. A. *J. Am. Chem. Soc.* **2003**, *125*, 7629−7640 and references therein.

(7) MeOH partial oxidation: Sato, S.; Iijima, M.; Nakayama, T.; Sodesawa, T.; Nozaki, F. *J. Catal.* **1997**, *169*, 447−454 and references therein.

(8) MeOH oxidative carbonylation: Anderson, S. A.; Root, T. W. *J. Catal.* **2003**, *217*, 396−405 and references therein.

(9) For a review of grafting methods, see Che, M.; Louis, C. In *Preparation of Solid Catalysts*; Knözinger, H., Weitkamp, J., Eds.; Wiley-VCH: Weinheim, Germany, 1999; pp 341−355.

(10) Zhao, D.; Feng, J.; Huo, Q.; Melosh, N.; Fredrickson, G. H.; Chmelka, B. H.; Stucky, G. D. *Science* **1998**, *279*, 548−552.

(11) Terry, K. W.; Lugmair, C. G.; Gantzel, P. K.; Tilley, T. D. *Chem. Mater.* **1996**, *8*, 274−280.

(12) Tsuda, T.; Hashimoto, T.; Saegusa, T. *J. Am. Chem. Soc.* **1972**, *94*, 658−659.

(13) Calculated for materials after loss of the organics upon heating. Elemental analyses for Cu content: **CuOSi/SBA(5.0)**, 5.21%; **CuOSi/SBA(3.5)**, 3.61%; **CuOᵗBu(5.0)**, 4.31%; **CuOᵗBu(3.5)**, 3.35%.

(14) (a) Terry, K. W.; Tilley, T. D. *Chem. Mater.* **1991**, *3*, 1001−1003. (b) Terry, K. W.; Lugmair, C. G.; Tilley, T. D. *J. Am. Chem. Soc.* **1997**, *119*, 9745−9756. (c) Fujdala, K. L.; Tilley, T. D. *Chem. Mater.* **2001**, *13*, 1817−1827. (d) Fujdala, K. L.; Tilley, T. D. *J. Am. Chem. Soc.* **2001**, *123*, 10133−10134. (e) Fujdala, K. L.; Tilley, T. D. *Chem. Mater.* **2002**, *14*, 1376−1384. (f) Lugmair, C. G.; Fujdala, K. L.; Tilley, T. D. *Chem. Mater.* **2002**, *14*, 888−898.

(15) The hydroxyl concentration of the SBA-15 was determined to be 1.3(1) "OH" nm⁻², by titration with Mg(C₆H₅CH₂)₂•2THF and quantification of the toluene evolved by ¹H NMR spectroscopy, in accordance with known procedures (refs 14d,f).

(16) For example, uncalcined: **CuOSi/SBA(3.5)**, 678 m² g⁻¹ and 0.88 cm³ g⁻¹; **CuOSi/SBA(5.0)**, 567 m² g⁻¹ and 0.80 cm³ g⁻¹; **CuOᵗBu(5.0)**, 745 m² g⁻¹ and 0.98 cm³ g⁻¹. After heating: **CuOSi/SBA(3.5)**, 800 m² g⁻¹ and 1.01 cm³ g⁻¹; **CuOSi/SBA(5.0)**, 782 m² g⁻¹ and 1.04 cm³ g⁻¹; and **CuOᵗBu/SBA(5.0)**, 813 m² g⁻¹ and 1.09 cm³ g⁻¹.

(17) See the Supporting Information for details.

(18) (a) Tranquada, J. M.; Heald, S. M.; Moodenbaugh, A. R. *Phys. Rev. B* **1987**, *36*, 5263−5274. (b) Nguyen, H. T.; Nakagawa, K. H.; Hedman, B.; Elliott, S. J.; Lidstrom, M. E.; Hodgson, K. O.; Chan, S. I. *J. Am. Chem. Soc.* **1996**, *118*, 12766−12776.

(19) (a) Frenkel, A. I. *J. Synchrotron Radiat.* **1999**, *6*, 293−295. (b) Nashner, M. S.; Frenkel, A. I.; Somerville, D.; Hills, C. W.; Shapley, J. R.; Nuzzo, R. G. *J. Am. Chem. Soc.* **1998**, *120*, 8093−8101.

(20) Montano, P. A.; Shenoy, G. K.; Alp, E. E.; Schulze, W.; Urban, J. *Phys. Rev. Lett.* **1986**, *56*, 2076−2079.

JA048701+